Durable lubricant-infused anodic aluminum oxide surfaces with high-aspect-ratio nanochannels

Wu, Dequan; Zhang, Dawei; Ye, Yuwei; Ma, Lingwei; Minhas, Badar; Liu, Bei; Terryn, Herman A.; Mol, Johannes M.C.; Li, Xiaogang

DOI
10.1016/j.cej.2019.02.163

Publication date
2019

Document Version
Final published version

Published in
Chemical Engineering Journal

Citation (APA)
Wu, D., Zhang, D., Ye, Y., Ma, L., Minhas, B., Liu, B., Terryn, H. A., Mol, J. M. C., & Li, X. (2019). Durable lubricant-infused anodic aluminum oxide surfaces with high-aspect-ratio nanochannels. *Chemical Engineering Journal*, *368*, 138-147. https://doi.org/10.1016/j.cej.2019.02.163

Chemical Engineering Journal 368 (2019) 138–147

Contents lists available at ScienceDirect

Chemical Engineering Journal

journal homepage: www.elsevier.com/locate/cej

Durable lubricant-infused anodic aluminum oxide surfaces with high-aspect-ratio nanochannels

Dequan Wu[a], Dawei Zhang[a,*], Yuwei Ye[a], Lingwei Ma[a], Badar Minhas[a], Bei Liu[a], Herman A. Terryn[b], Johannes M.C. Mol[c], Xiaogang Li[a]

[a] Beijing Advanced Innovation Center for Materials Genome Engineering, Institute for Advanced Materials and Technology, University of Science and Technology Beijing, Beijing 100083, China
[b] Department of Materials and Chemistry, Research Group Electrochemical and Surface Engineering, Vrije Universiteit Brussel, Brussels, Belgium
[c] Department of Materials Science and Engineering, Delft University of Technology, Delft, The Netherlands

HIGHLIGHTS

- Lubricant was infused into high-aspect-ratio AAO nanochannels by vacuum impregnation.
- LIS provided long-term corrosion resistance due to the high lubricant-storing capacity.
- LIS demonstrated self-healing effects over surface cracks and wear damages.
- Cryo-SEM was used to directly observe the lubricant infusion and self-healing action.

GRAPHICAL ABSTRACT

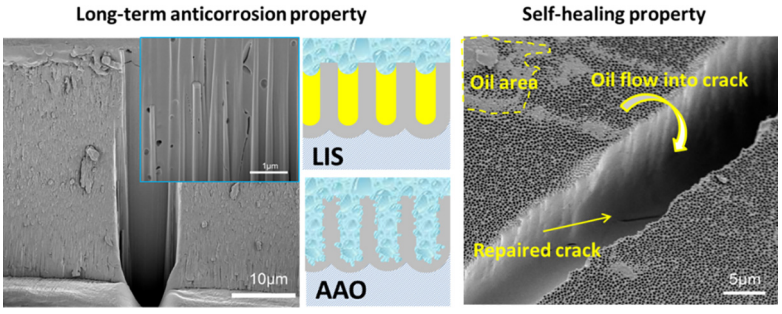

ARTICLE INFO

Keywords:
Lubricant-infused surface
Self-healing
Corrosion
Anodic aluminum oxide
Wear

ABSTRACT

Recently, lubricant-infused surfaces (LIS) have emerged as a prominent class of surface technology for anti-fouling, anti-icing and anticorrosion applications. However, long-term corrosion exposure and mechanical damages may deteriorate the practical performance of LIS during application. In this study, a robust LIS was fabricated by the vacuum impregnation of mineral oil into anodized aluminum oxide (AAO) nanochannels with a depth of 50 μm. The impregnation of the lubricant through the entire depth of the high-aspect-ratio nanochannels was visualized under cryo-scanning electron microscopy (cryo-SEM) and also confirmed by weight gain measurements. Electrochemical impedance spectroscopy (EIS) and potentiodynamic polarization (PDP) tests showed that the lubricant stored in the deep nanochannels of LIS can provide excellent corrosion protection during long-term immersion. Furthermore, the as-prepared LIS demonstrated superior resistance to mechanical damage due to a self-healing effect by the lubricant. As shown by cryo-SEM observation and PDP tests, the microcracks formed on the LIS can be instantaneously repaired by the in-flow of the oil from the surrounding surface. In the tribological tests, the LIS also presented high wear resistance and superior mechanical durability.

1. Introduction

The development of advanced surface technologies to prevent the corrosion of metals is of high research interest and industrial importance [1]. Bionic coatings developed by mimicking the surface morphology and chemistry of plants and animals have received much

* Corresponding author.
E-mail address: dzhang@ustb.edu.cn (D. Zhang).

https://doi.org/10.1016/j.cej.2019.02.163
Received 23 November 2018; Received in revised form 20 February 2019; Accepted 22 February 2019
Available online 23 February 2019
1385-8947/

attention to enhance the barrier performance of the surfaces against corrosion attacks [2–4]. Inspired by *Nepenthaceae*, micro- or nanoporous substrates have been used to lock low-surface-energy lubricating liquids to form liquid-solid composite surfaces, which were defined as lubricant-infused surfaces (LIS) [5]. A LIS is typically fabricated by replacing the air entrapped in a surface microstructure with a lubricating liquid [6,7]. The following criteria should be met when designing a LIS: i) the lubricant must wet and stably adhere within the substrate; ii) the lubricant is immiscible with other contacting fluids in the service environments; and iii) the contacting fluid does not penetrate into the substrate [5]. To satisfy these requirements, rough substrates with chemical stability and complete wettability with the lubricant are often used. And the lubricant should be locked inside the porous substrate by capillary forces and immiscible to external aqueous media from the environment [8–10]. The durability of LIS is typically attributed to the nature of the porous substrates, the stability of the lubricants and the interaction between substrate, lubricant and external liquid [11,12]. These liquid-solid composite surfaces exhibit superior water-repelling and self-healing abilities, which are both important for long-term corrosion protection [13,14].

Despite the outstanding lubricant property of LIS, few studies have considered its mechanical durability and longevity [15–17]. To date, most LIS are prepared by simply infusing lubricants into the micro/nanopores of superhydrophobic surfaces [18]. For example, some of the most common LIS substrates include porous fabric/fibers [19], self-assemblies [20], and hierarchical micro/nanoparticles [21]. Because of the delicate and often brittle features of the porous structures [22–24], these substrates suffer from low mechanical durability and may lose their protective and lubricating properties as results of cracking and wear in harsh service environments [25]. Additionally, the liquid stored in the porous substrate is prone to diffuse out due to its high mobility [26–29]. Therefore, the substrates with shallow micro/nanopores which possess low liquid-storing capacity may only possess limited longevity for corrosion protection.

In view of these issues, substrates with high porosity and also high mechanical rigidity are being sought for the preparation of durable LIS [30–32]. Anodization of aluminum, which creates hard and rigid oxide films [33,34], is considered to be one of the most widely used methods for improving the wear and corrosion resistance of aluminum surfaces [35,36]. In addition, the orderly arrangement of nanochannels in the anodized aluminum oxide (AAO) make them good containers for lubricant infusion and the infusion depths can be easily controlled by the thickness of the AAO film [37]. However, it is a great challenge to completely fill the deep and narrow nanochannels considering their high aspect ratio and dead-end structure in nanoscale. So far, only few researches have infused lubricants in AAO surfaces [38–41]. These studies typically used AAO with a thickness of hundred nanometers to several microns, and thicker AAOs with deep lubricant infusion have not been reported.

In this paper, we aim to fabricate durable LIS by infusing lubricating mineral oil into the high-aspect-ratio AAO nanochannels. The mineral oil was selected as the infused lubricant because of its desirable chemical properties and balanced performance such as substrate wettability, liquid immiscibility, chemical inertness, and minimal cloaking effect on water droplets deposited on the LIS surface [18]. A ~50 μm thick AAO nanoporous surface was employed for the first time to enhance the mechanical robustness of the LIS against physical damage. The high-aspect-ratio nanochannels also serve as deep reservoirs to store a large amount of lubricant, which warrants long-term anticorrosion performance and an instantaneous self-healing effect over the damage. To overcome the challenge of infusing the lubricant into the high aspect ratio nanochannels, a vacuum impregnation method was adopted using a homemade instrument (Scheme 1). Compared to other common LIS fabrication methods (e.g., direct immersion or spin coating), the vacuum impregnation method can create a high negative pressure to facilitate the capillary wetting of the lubricant into the inner oxide pore.

The extent of oil infusion was confirmed by cryo-scanning electron microscopy (cryo-SEM) observation and weight measurements. The wettability of different surfaces was studied by water contact angle and sliding measurements. To investigate the long-term corrosion resistance, the obtained surfaces were tested by electrochemical impedance spectroscopy (EIS) during the immersion into a 1 M NaCl solution for over 80 days, and the loss of lubricant was also tracked by direct observation using cryo-SEM. Moreover, the ability of the LIS to heal over surface cracks was studied by cryo-SEM. The self-healing action of the LIS was further evaluated by potentiodynamic polarization (PDP) tests in a 1 M NaCl solution, as well as measuring the depth and topography of the wear track and tribo-electrochemical properties under wear conditions.

2. Experimental section

2.1. Materials

High-purity aluminum foils (25 mm × 25 mm × 0.2 mm, 99.999% purity) were purchased from the Beijing Institute of Nonferrous Metals. The lubricant used in this study was a mineral oil obtained from Shell (Shell Advanced AX5). The fluoroalkyl silane (1H,1H,2H,2H-perfluorodecyltriethoxysilane, 97%) was purchased from Sigma-Aldrich. All other chemicals and solvents were purchased from Sinopharm.

2.2. Fabrication of the LIS

To prepare the AAO, the aluminum foil was first degreased by sonication in ethanol and subsequently electro-polished at 20 V for 2 min in a mixed solution of 80 vol% ethanol and 20 vol% perchloric acid at 5 °C. Afterwards, the aluminum foil was washed with ethanol and dried by nitrogen gas. The AAO nanoporous surface was fabricated by a two-step anodization process. The first anodization was performed at 195 V via a DC source (Keysight, N8741) using electro-polished aluminum foil as the anode and degreased aluminum foil as the cathode. Both electrodes were immersed in a 0.3 M phosphoric acid solution at 5 °C with an exposed electrode area of 25 mm × 25 mm. The solution was magnetically stirred at 300 rpm to avoid local overheating. After anodization for 60 min, the first anodized layer was removed by etching in an aqueous solution containing 6 wt% phosphoric acid and 1.8 wt% chromic acid at 60 °C for 15 min. The second anodization was then performed under the same conditions as the first one for 2 h.

The prepared AAO sample was infused with oil by a homemade device (Scheme 1a). The device was composed of a cylindrical container (where the specimen was placed) connected to a vacuum pump (to achieve a low vacuum of ~3 Pa), an air-exhaling valve, an air-inlet valve, and an oil-inlet valve (to regulate the oil flow). Before the oil impregnation process, the AAO surface was first cleaned with acetone in an ultrasonic bath for 10 min and dried. The lubricating oil was vacuumed for 20 min to expel the dissolved air, and the cleaned AAO surface was fixed in the sample container. With the exhaling valve open and the air-inlet valve closed (Scheme 1b), the container was vacuumed for 5 h to completely remove the air in the container and in the AAO nanochannels (Scheme 1c). Subsequently, the oil-inlet valve was opened to allow the oil to flow into the container under a negative pressure (Scheme 1d) and submerge the AAO sample. The oil-inlet valve was then closed, and the sample was soaked in the oil under vacuum to eliminate the air from the oil injection step and drive the infiltration of the lubricant into the nanochannels. After soaking for 1 h, the air-inlet valve was opened to allow air to flow into the container. The pressure difference between the inner nanochannels and the atmosphere outside also helped to force the lubricant to deeply infuse into the nanochannels (Scheme 1e). In the last step, the sample surface was tilted at 45° for 5 min to remove the excess lubricant on the surface. To demonstrate the oil-infusing efficiency by the vacuum impregnation

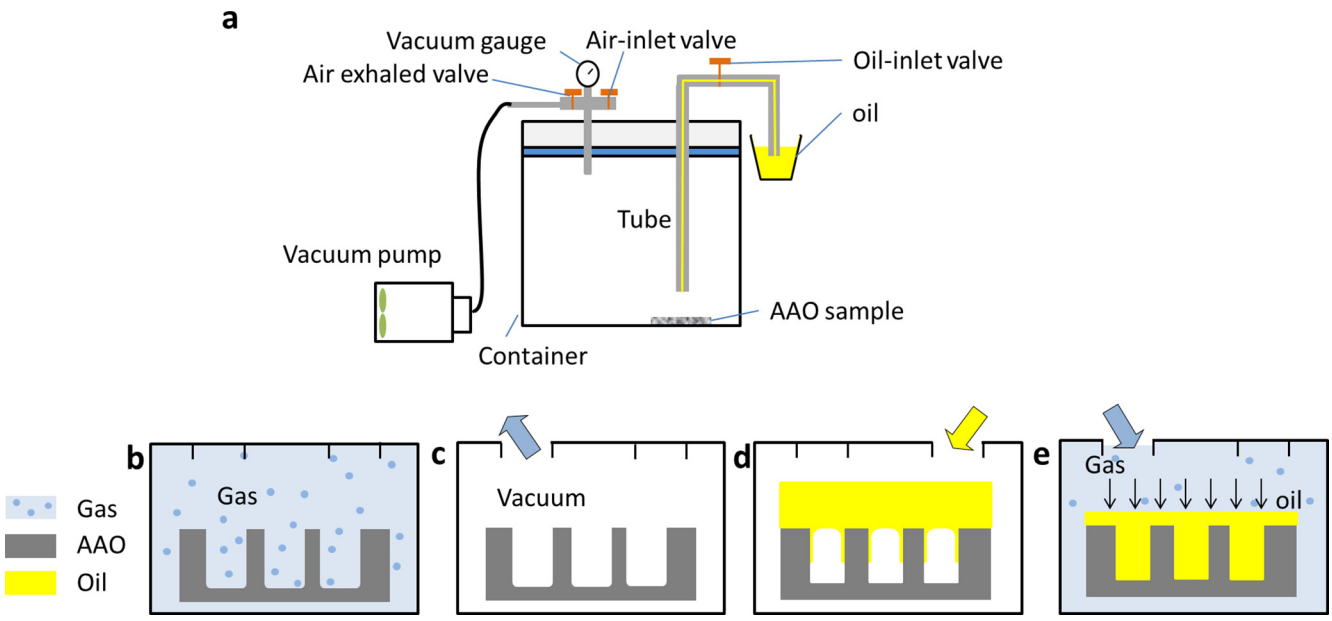

Scheme 1. The lubricant impregnation procedure using a homemade device as shown in (a); (b) the sample is placed in the container; (c) the air is pumped out from container and nanochannels; (d) oil is injected into container and covers the surface of the sample; (e) the container is refilled with air which further facilitates the oil infusion.

method, we also attempted to prepare the lubricant-infused surface (LIS) by simply immersing the AAO specimen in oil under ambient atmospheric pressure. To further improve the surficial hydrophobicity of LIS, the prepared AAO was modified with hydrophobic molecules prior to lubricant impregnation. The AAO samples were immersed in fluoroalkyl silane solution (1 vol% fluoroalkyl silane, 8 vol% deionized water and 91 vol% ethanol) for 30 min. Then the samples were taken out and heated at 150 °C for 60 min, followed by the lubricant impregnation procedures as depicted in Scheme 1.

2.3. Cryo-SEM

Cryo-SEM (FEI Helios NanoLab G3 UC) was performed to observe the LIS specimens at microscopic resolution. Specifically, the LIS specimen was embedded into a copper holder with conductive glue and mounted in a cryo-cell holder. The cryo-cell was plunged into a liquid nitrogen trough to freeze the specimens. After submerging in liquid nitrogen for ~10 s, the specimen was bent carefully by tweezers to break off and expose a fresh cross section. The cryo-cell was then transferred into the sample chamber and sublimated at −90 °C for 25 min to remove the ice crystals formed on the specimen surface during the freezing process in the liquid nitrogen. The cryo-SEM observation chamber was maintained at a temperature of −140 °C under a vacuum of ~1.02×10^{-5} Pa. To improve the surface conductivity, all specimens were sputter coated with gold at 10 mA current for 60 s. To obtain a smooth cross-section, the LIS was milled inside the cryo-SEM chamber by the focus ion beam (FIB) with a beam energy of 30 keV, a current of 2.5 nA, and a dwell time of 100 ns per pixel. After the FIB process, the sample was transferred to a spraying chamber to sputter with gold again. The SEM images were acquired by using either secondary or back-scattered electrons (2 keV, 60 pA).

2.4. Surface wettability

Static contact angle and sliding angle measurements (Dataphysics OCA20) were performed to check the surface wettability of the specimens. The static contact angles were measured by placing a sessile deionized water droplet (~5 μL) or oil (~5 μL) onto the AAO and LIS sample surfaces. The sliding angle (SA) was recorded by tilting the surface slowly until a 10 μL water droplet could slide off. The results were the average values from five measurements on different areas of the samples. The T-test was performed to check the P value of each data set.

2.5. UV/Vis spectroscopy

UV/Vis spectroscopy (HITACHI U3900H) was conducted to detect the quantity of oil remained in the LIS samples. Firstly, the correlation between the peak intensity of UV spectra and the concentration of lubricant in dichloromethane was established by measurements performed with standard concentrations of the mineral oil in dichloromethane. To determine the quantity of the mineral oil in the nanochannels, the LIS specimens were submerged in 5 mL dichloromethane for 1 h under ultrasonication for extraction.

2.6. Electrochemical tests

EIS and PDP tests were performed using a PARSTAT 2273 electrochemical station in a three-electrode cell in a 1 M NaCl solution at 25 °C. The working electrode, the counter electrode and the reference electrode were the LIS (or bare AAO) sample, platinum foil and saturated calomel electrode (SCE), respectively. Before the EIS and PDP measurements, the sample was immersed in the electrolyte for ~10 min until the open-circuit potential (OCP) was stable. The EIS experiments were performed over frequency range from 10^5 to 10^{-2} Hz with an amplitude of 20 mV. Polarization curves were recorded over a scanning range of ± 500 mV around the OCP value, and the potential sweep rate was 3 mV s^{-1}. All tests were performed at least twice to verify the reproducibility.

2.7. Tribo-electrochemical tests

The wear resistance of the bare AAO and LIS was evaluated using a ball-on-disk type tribo-electrochemical tester (RETC MFT5000) in a 1 M NaCl solution. In the test, a stainless-steel ball (diameter ~6 mm) was pressed against the specimen surface (10 mm × 10 mm) under a constant load of 5 N at a speed of 20 mm/s for 1800 s. The sliding stroke was 5 mm. A three-electrode system was used, including the specimen

as the working electrode, a saturated calomel electrode (SCE) as the reference electrode, and a Pt foil as the counter electrode. The wear depth, friction coefficient and OCP were recorded *in situ* during the sliding in the electrolyte. Then, EIS and PDP tests were performed under the same sliding conditions. After the tribo-electrochemical test was finished, the morphology of the worn area was observed by confocal laser scanning microscope (CLSM, Keyence VK-X).

3. Results and discussion

In this paper, the LIS was fabricated by impregnating the dead-end nanochannels (diameter ~200 nm; depth ~50 μm) with a mineral oil. As described in the Supporting Information, the interaction between the solid substrate, lubricant and external liquid (water) was analyzed to rationalize the LIS design in this study. To compare the level of infusion into the high-aspect-ratio nanochannels, both vacuum impregnation and ambient-pressure direct immersion were carried out. The oil tends to spread in the AAO nanochannel attributing to the low surface tension of oil [42–44]. However, under ambient-pressure immersion, the air trapped inside the nanochannels can resist the continuous infusion of the lubricant. Therefore, as depicted in Scheme 1, a vacuum condition was created in this study to remove the trapped air, ensuring the deep lubricant infusion into the high aspect ratio nanochannels.

Due to the high mobility of the liquid lubricant, direct observation of the LIS by conventional SEM or optical microscopes is challenging. To solve this problem, previous studies have tried introducing cross-linking agents and solidifying the lubricant in order to verify the infusion condition with SEM [38]. In this study, cryo-SEM, which was developed to study biological samples with high moisture contents, was used for the first time to provide an *in situ* observation of the frozen lubricant in the nanochannels [45]. To prevent the escape of the lubricant, the LIS specimen was freeze-fractured in liquid nitrogen at −140 °C and subsequently milled by FIB in the cryo-SEM chamber to reveal a smooth cross-sectional morphology. Fig. 1a shows the cross-sectional morphology of the untreated AAO, which contains well-aligned empty nanochannels. After immersing in the lubricant at ambient pressure for ~12 h, it was found that the lubricant covered the surface on top of the pores but could not penetrate inside (Fig. 1b). Nevertheless, for the LIS prepared by vacuum impregnation, the pores were infused with the lubricant throughout the entire depth (Fig. 1d). At higher magnification, the lubricant oil was observed to fill in the area between the pore walls, and a few small air pockets were observed in the oil column (Fig. 1e). Even the bottom of the nanochannels was fully infused with the lubircant, as it shown in Fig. 1f. The cryo-SEM observation further confirms that the vacuum impregnation method developed in this study possesses a considerably improved capability of filling oils into the high-aspect-ratio nanochannels. The filling efficiencies of the two methods were also experimentally verified by weighing the AAO samples before and after the impregnation process (Table S2). The depth of oil infusion under vacuum conditions attained ~49 μm, approaching the full thickness of the nanochannels. In contrast, the infused oil reached to a depth of only ~6 μm after simple immersion.

The wettability of the bare AAO, the LIS and the fluoroalkyl-silane-treated LIS was studied by static contact angle and sliding angle measurements (Fig. 2). The water contact angles on the fresh aluminum surface and the bare AAO were 50.4° and 68.0°, respectively. The contact angle of the lubricant on the AAO surface was lower (~40.2°) than that of water on the AAO, suggesting that the AAO had a better affinity with the lubricant than water [46]. The water droplet on the LIS and the fluoroalkyl-silane-treated LIS exhibited a contact angle of 99.5° and 122.6°, respectively, which were both significantly higher than that on the bare AAO. The sliding processes of water droplets on the LIS and the fluoroalkyl-silane-treated LIS samples were recorded as shown in Fig. 2b-c.

As shown in Fig. 2b, the water droplet gradually slid off from the LIS specimen, indicating its water dewetting property. In comparison, the water droplet slid off immediately when it contacted the fluoroalkyl-silane-treated LIS, suggesting an enhanced surface hydrophobicity. Thus, compared to the hydrophilic AAO surface, which offers a low resistance to the wetting by aqueous corrosive media, the LIS and the fluoroalkyl-silane-treated LIS specimens presented an improved water repellency.

The durability of the LIS specimen was first assessed by studying its long-term corrosion resistance under aqueous immersion in a 1 M NaCl solution for up to 85 days. Fig. 3a-c and 3d-f are the EIS results for the bare AAO and LIS (50 μm thick), respectively. According to previous studies [47–49], the medium to high frequencies of the EIS spectra correspond to the outer porous layer of the AAO, whereas the low-frequency region mainly reflected the properties of the inner barrier layer of the AAO [50,51]. As shown in Fig. 3a, the capacitive loops of the Nyquist plots became smaller with immersion time, suggesting a decreased corrosion resistance. The impedance modulus at 0.01 Hz ($|Z|_{0.01Hz}$) of the Bode plots has also been commonly used as a good indicator of the corrosion resistance [52,53]. In Fig. 3b, the value of $|Z|_{0.01Hz}$ for the bare AAO was as high as $\sim 2 \times 10^8\ \Omega\,cm^2$ at the beginning of immersion but gradually decreased to $\sim 4 \times 10^7\ \Omega\,cm^2$ after 85 days of immersion, reflecting the barrier layer being attacked by penetrated corrosive solution [54,55]. The phase angles of bare AAO in Fig. 3c exhibited one time constant at the beginning of the immersion (i.e. 0 day), but demonstrated a second time constant corresponding to the corrosion of the barrier layer after immersion [55]. At lower frequencies, the phase angles continued to decrease during the immersion. The EIS results were further quantitatively analyzed by fitting with electrical equivalent circuits in Fig. S3a and b, for AAO at the beginning of immersion (i.e. 0 day) and after immersion for 3–85 days, respectively. As summarized in Table S3, the significant decreases in R_{ct} and R_b both suggested the deterioration of the barrier layer of the AAO under NaCl immersion.

According to Fig. 3d-f, the lubricant-infused AAO exhibited much more stable corrosion resistance under the long-term immersion. During the entire 85 days, the low-frequency regions of the Bode plots overlapped with their $|Z|_{0.01Hz}$ values remaining at $\sim 4 \times 10^8\ \Omega\,cm^2$, indicating a stronger protective performance than that of the bare AAO. Compared with the bare AAO, the LIS sample showed much different behavior during the initial stage of immersion in the high-frequency region where a distinct time constant was visible (Fig. 3e-f). In previous studies, similar observations were reported for AAOs that were sealed by hydrothermal methods or by chemical deposition [47–56]. Therefore, we postulate that the high-frequency region of the Bode plot reflected the lubricant layer (covered on surface and infused in pores), and the low-frequency region reflected the inner barrier layer. In Fig. 3e, the $|Z|$ values in the high-frequency plateau region slightly decreased within the first three days of immersion. This process reflected the gradual loss of the excess surface-adhered lubricant layer under an immersion environment (Scheme 2b), which was also verified by cryo-SEM observation of the cross section of the LIS specimen (Fig. 4a). The original thin lubricant layer adhered on the LIS specimen disappeared due to the slow but inevitable diffusion between oil and water and also the perturbation during the test [18]. However, in the Bode plots of LIS (Fig. 3e), a small plateau in high frequency was still visible after 10 days of immersion, which suggests that the oil columns infused in the deep nanochannels could still provide a strong and durable isolation between the aluminum substrate and the aqueous solution (Scheme 2c). After immersion for 85 days, only ~3 μm of the infused lubricant was lost (Fig. 4b) with most of the remaining lubricant well trapped in the nanochannels to resist further penetration of NaCl solution. According to previous study, the solubility of mineral oil in water was generally less than ~0.2 mg/mL[57]. As determined by UV/Vis spectroscopy, ~1.22 mg of the oil leached out from LIS surface and nanochannels after 85 days of immersion. The EIS results in Fig. 3d-f were fitted using the equivalent circuits in Fig. S3c-d. According to

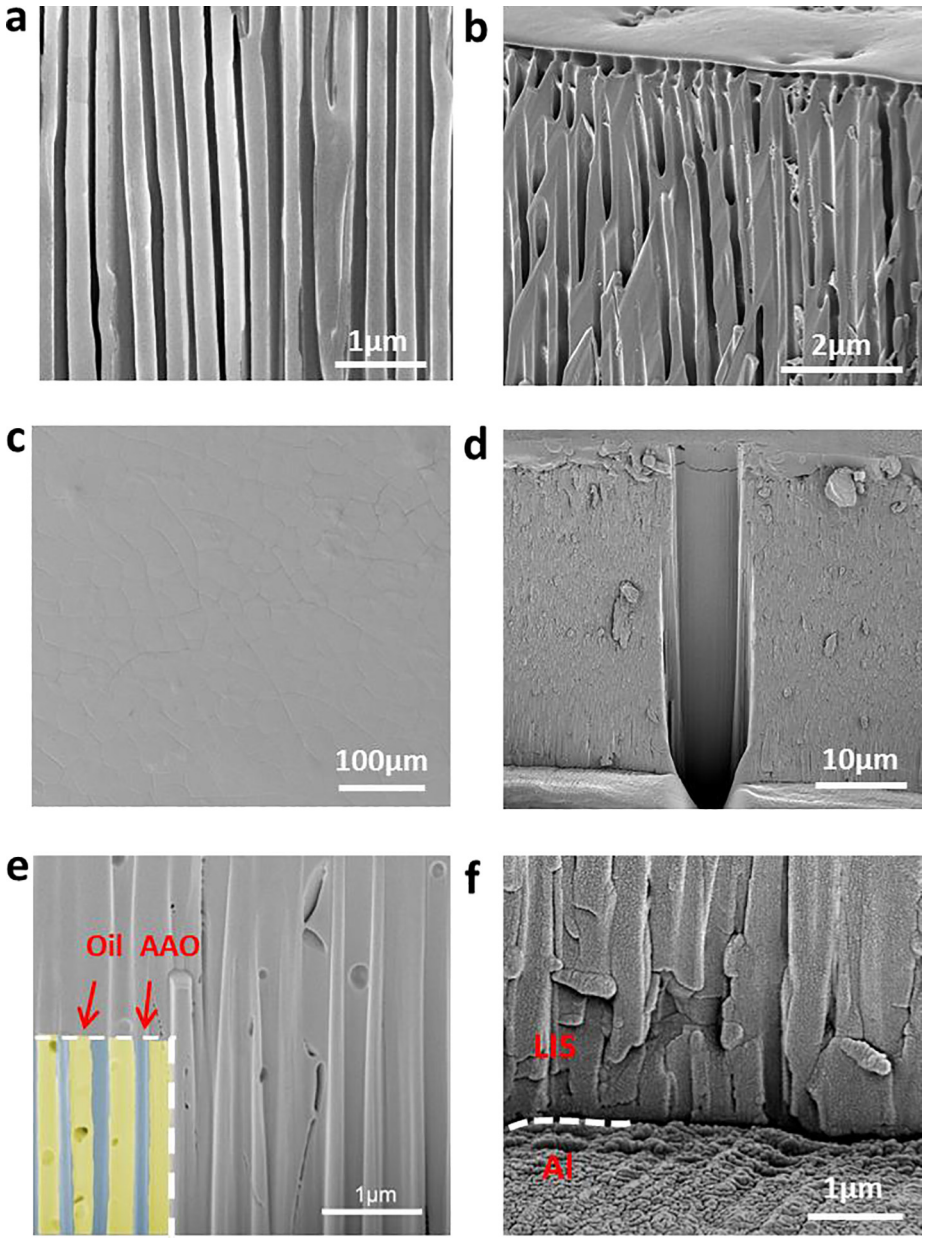

Fig. 1. Cryo-SEM images of the cross sections of (a) empty nanochannels of AAO and (b) pores of AAO after simple immersion; (c) top view of LIS; (d) full cross section of FIB-milled LIS fabricated by vacuum impregnation; (e) magnification of the oil infused nanochannels; (f) magnification of the boundary between the oil infused nanochannels and the aluminum substrate.

Table S3, although R_p decreased during the immersion reflecting the leaching of the mineral oil, R_b remains relatively stable, confirming that the barrier layer was well protected.

To demonstrate the advantage of high-aspect-ratio nanochannels in achieving durable corrosion protection, the LIS samples were also prepared using thin AAOs with a thickness of 5 μm and were tested by EIS under the same conditions (Fig. S2). Like the thick LIS, the high-frequency |Z| values in the Bode plots for thin LIS slightly decreased at the initial stage of immersion, which was attributed to the loss of the surface-adhered oil layer. However, in contrast to the stable corrosion resistance of the thick LIS, a much more substantiated decrease in the low-frequency |Z| values was observed for the thin LIS during the 85 days of immersion. It shows that the high-aspect-ratio nanochannels in the thick AAO containing more oil can provide a more durable corrosion protection.

The corrosion resistance of the bare AAO and the lubricant-infused AAO surfaces were also investigated by PDP tests in a 1 M NaCl solution (Fig. 5). The corrosion current density of the bare AAO was $\sim 1.53 \times 10^{-8}$ A cm^{-2}. The infusion of lubricant significantly suppressed both the anodic and cathodic reactions of the corrosion process underneath the AAO layer. The corrosion current density of the lubricant-infused AAO was $\sim 2.99 \times 10^{-10}$ A cm^{-2}, which was almost two orders of magnitude lower than that of the bare AAO. These results further proved that the infusion of liquid lubricant offers better corrosion inhibition than the entrapment of air in the nanochannels.

Because of the brittle nanoporous structure, the AAO surface is vulnerable to cracking and wear under severe mechanical impacts, which may significantly reduce its corrosion resistance. To evaluate the damage tolerance of the LIS, artificial surface cracks were prepared by bending the specimen around a 1 cm diameter cylinder rod, followed by immersion into a 1 M NaCl solution for the PDP assessment. In the case of the bare AAO, the corrosion potential after cracking decreased from −1.12 to −1.26 V (vs. SCE), and the corrosion current density increased from $\sim 1.53 \times 10^{-8}$ to $\sim 6.78 \times 10^{-8}$ A cm^{-2}. Such an

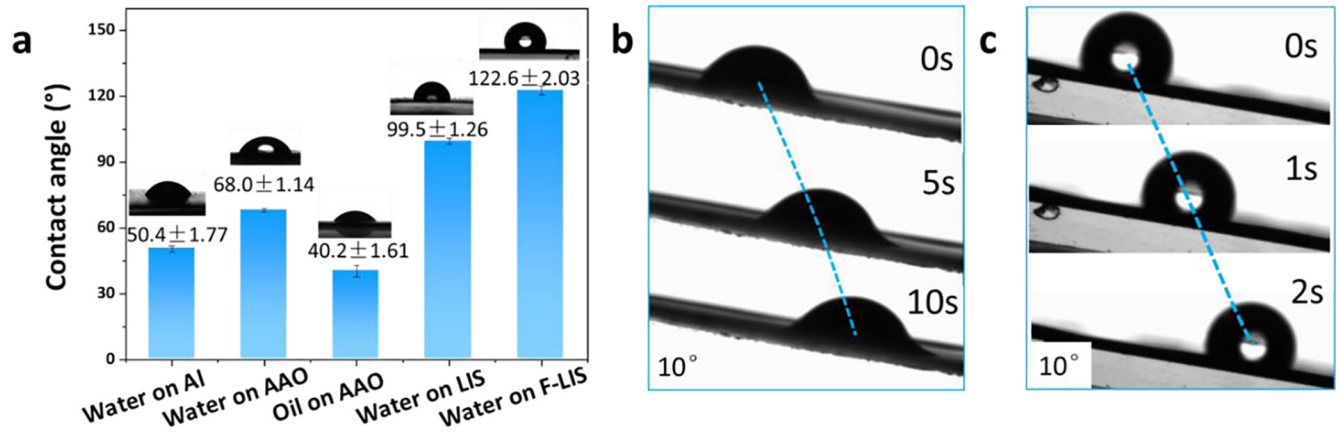

Fig. 2. (a) Contact angles of liquid droplets (water and oil, 5 μL) on the bare AAO and LIS. Sliding process of a water droplet (10 μL) on (b) LIS and (c) fluoroalkylsilane-treated LIS at a sliding angle of 10°. The T-test showed that P value < 0.05 for all contact angle data.

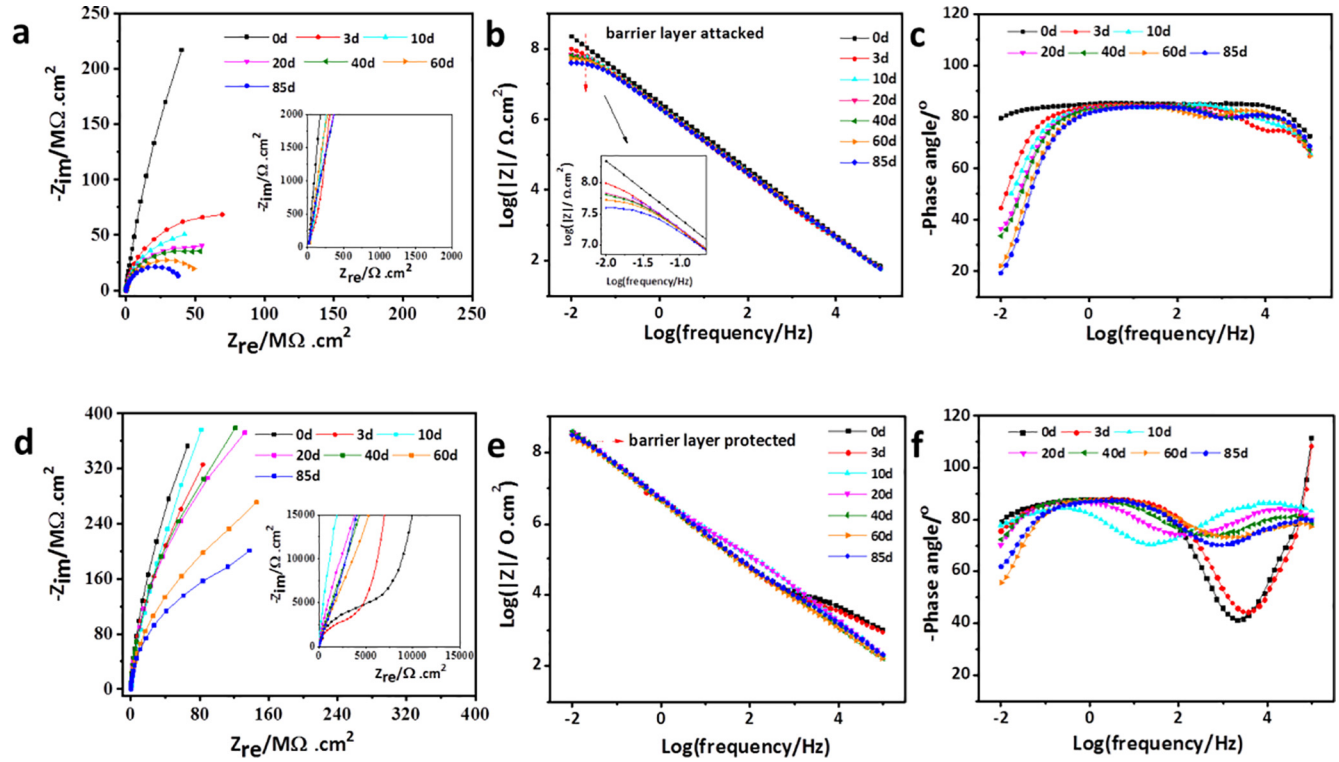

Fig. 3. Impedance spectra of (a–c) bare AAO and (d–f) LIS after 0, 3, 10, 20, 40, 60 and 85 days of immersion in 1 M NaCl solution. (a,d) Niquist plot; (b,e) Bode plot; (c,f) Phase angle plot.

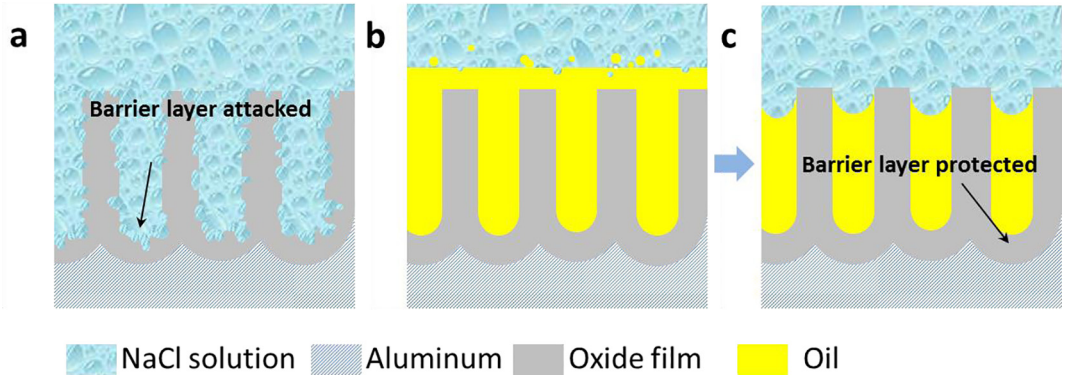

Scheme 2. (a) barrier layer of AAO attacked by penetrated corrosive solution; (b) dissolution of the oil layer adhered to LIS and (c) barrier layer protected by the remaining oil in the nanochannels.

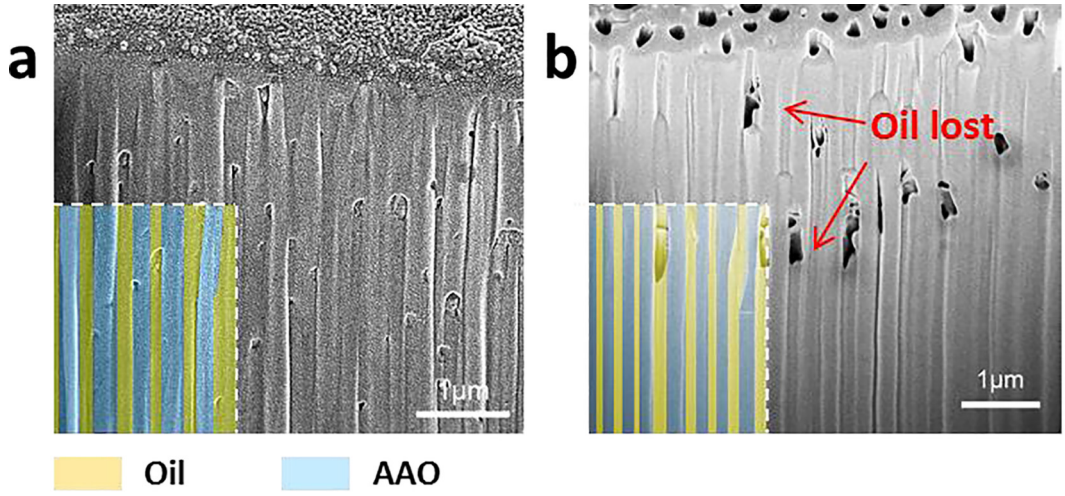

Fig. 4. Cryo-SEM image of LIS in different immersion stages: (a) upper lubricant layer dissolved after 10 days (b) ~3 μm thick lubricant lost in the nanochannels after 85 days.

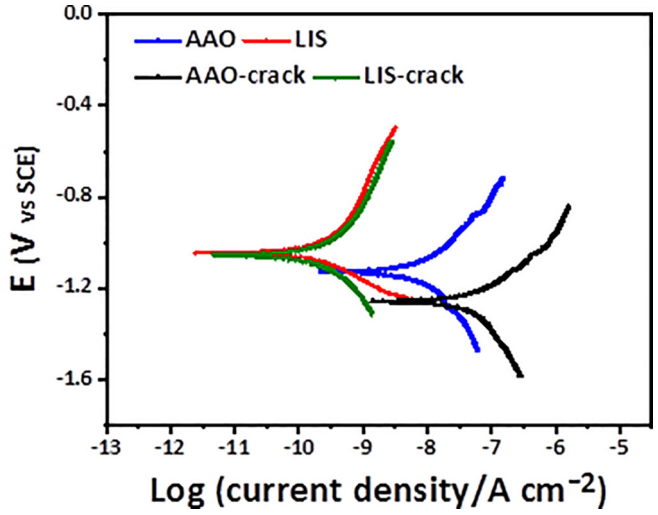

Fig. 5. Potentiodynamic polarization results for the intact and damaged samples (bare AAO and LIS).

increase in the corrosion rate can be attributed to the exposed fresh aluminum substrate within the cracks. In contrast, the corrosion potential of the cracked LIS remained almost the same as that of the intact LIS and the corrosion current density was only slightly higher (~3.95×10^{-10} A cm^{-2}). The cracking on the LIS instantaneously released the lubricant stored in the nanochannels, which covered the surface to form a protective lubricant layer on the exposed substrate, demonstrating a self-healing effect over the corrosion resistance. To generate wider cracks, the LIS samples were also bended around cylinder rods with a smaller diameter (5 mm) or folded. As shown in Fig. S4b, the polarization curves of the LIS bended around 5 mm diameter cylinder rod almost overlapped with that of the intact LIS. The corrosion current density of the folded LIS was only slightly higher, indicating the excellent self-healing property.

To highlight the self-healing efficiency of the lubricant stored in deep nanochannels, cracking was also produced on the thin AAO with a thickness of 5 μm and was tested under the same conditions. The result in Fig. S4a shows that the corrosion current density of the thin LIS (~3.67×10^{-10} A cm^{-2}) was similar to that of thick LIS. However, after cracking, the current density of the thin LIS increased remarkably to ~1.70×10^{-8} A cm^{-2}, which was two orders of magnitude larger than that of the thick ones. The thin porous AAO layer could not store sufficient lubricant oil to fully recover the corrosion resistance at the crack regions, demonstrating a poor self-healing efficiency.

The self-healing effect of the LIS specimen against cracking was also visually studied by the cryo-SEM images in Fig. 6a-d. The images of cracks on bare AAO were shown in supporting document (Fig. S5). As shown in Fig. 6b, the crack with a width of ~15 μm was filled with the lubricant. While most of the intact surface was covered with the lubricant, a relatively dry region with much less oil coverage can be found on the intact surface in the close vicinity of the cracks (Fig. 6b-e). These observations suggest that the repair of the crack also relies on the inflow of lubricant from the nanochannels in the surrounding intact surface to cover the exposed surface (Fig. 6f).

The self-healing ability of the LIS was also assessed under tribological conditions at a constant load of 5 N and a sliding speed of 20 mm/s for 30 min in a 1 M NaCl solution. Fig. 7a shows the coefficient of friction (CoF) during the wear test and the wear depth after testing. The CoF value reflects the maximum force to break the microscopic solid junctions between the sample surface and ball surface [37]. In Fig. 7a, the CoF value of the bare AAO increased at the beginning of sliding as the testing ball was in contact with the rough AAO surface and then stabilized at ~0.45 in the regular reciprocating motion. In contrast, the CoF of the LIS maintained a low value of ~0.12 during the entire test, which was attributed to the lubricant layer covering the rough porous surface. The infused lubricant forms a continuous liquid film that reduces the frictional force and protects the underlying AAO substrate. In Fig. 7b, the wear depth of the bare AAO was ~48 μm, which means the oxide layer was almost completely worn out after 30 min. In comparison, the LIS specimen shows a wear depth of only ~4.5 μm. These results are visually confirmed by the CLSM morphology of the worn surfaces of the bare AAO and LIS (Fig. 7d and e). The anodized film of the bare AAO was crushed into small pieces, while the LIS specimen remained relatively intact because of its low CoF and the self-healing action. The wear damage to the AAO nanochannels could release more lubricant, which repaired the defects to maintain a smooth surface and alleviated further damages. Compared to the thick LIS, Fig. S6 shows that the LIS prepared by the 5 μm thick AAO was completely worn out under the same test conditions, which highlights the benefit of using thick AAO substrate in the preparation of LIS. Fig. S7a-b demonstrated the wear resistances of the LIS under higher loads. From 5 to 12 N, the CoF values remained stable ~0.14, although the wear depths were progressively increased revealing the partial but permanent damage to the AAO film. When the friction load was increased to 14 N, the CoF significantly increased to 0.19 and the AAO film has been completely worn out.

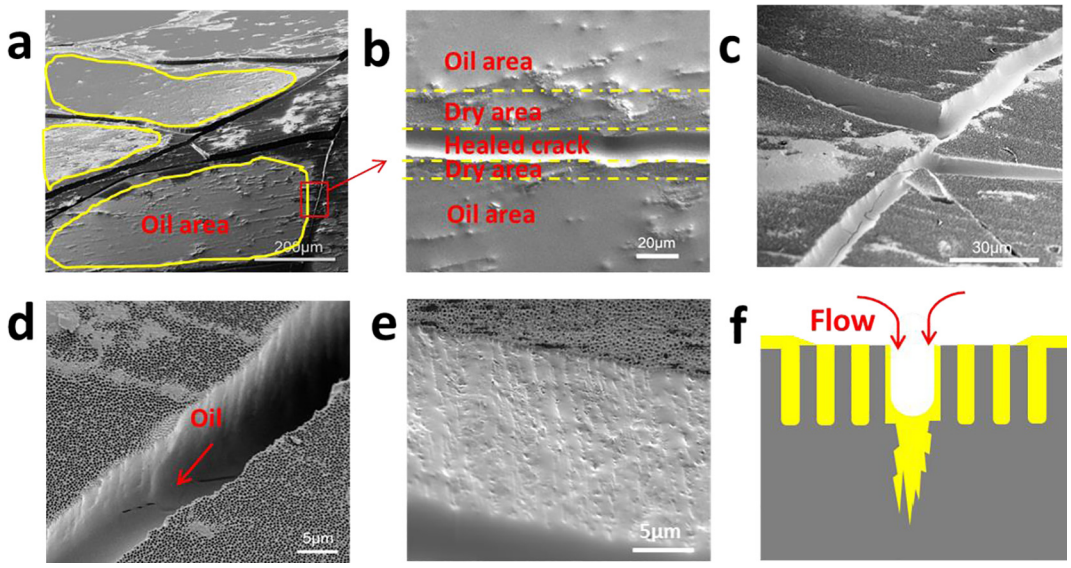

Fig. 6. Cryo-SEM images of (a-c) micro-cracks generated on the LIS and (d) LIS surface surrounding the micro-crack; (e) cross section of crack covered with lubricant (f) schematic illustration of the repairing process.

To further probe the self-healing process of the LIS under tribological conditions, the OCP values of the bare AAO and LIS were tracked before, during and after the wear process. It has been reported that the OCP in the wear process is a mixed potential originating from contributions of the active state of the material inside the wear track and the passive state of the unworn area outside the wear track [58]. As shown in Fig. 7c, much higher OCP values of the LIS are observed than that of the bare AAO during the entire testing period. When the wear started, the OCP values of bare AAO suddenly dropped to −1.1 V (vs. SCE), which was attributed to the destruction of the aluminum oxide layer [59]. After 1400 s, the OCP further decreased to −1.28 V (vs. SCE), which may be caused by the exposure of aluminum substrate. When the wearing process ended, the OCP of the bare AAO gradually increased to ~ −1.04 V (vs. SCE), which may be attributed to the oxidation of the exposed aluminum substrate. However, because of the permanent wear damage, the final OCP value was still much lower than that of the intact surface. In contrast, the OCP value of the LIS specimen was only slightly reduced after the wear test began and well remained at ~ −0.73 V (vs. SCE) during the entire test. The reduction in the OCP was mostly likely resulted from the perturbation by the sliding motion. After the wear test stopped, the OCP value recovered to its original value. The superior mechanical durability of the LIS may be attributed to the sufficient lubrication and efficient self-healing property. When tested at a higher frictional load, as it shown in Fig. S7c, a decreased OCP (under wearing) was observed especially at the latter stage of the wear test. Nevertheless, when the test stopped, the OCP values of all cases recovered as the result of the healing effect by the in-flowed lubricant.

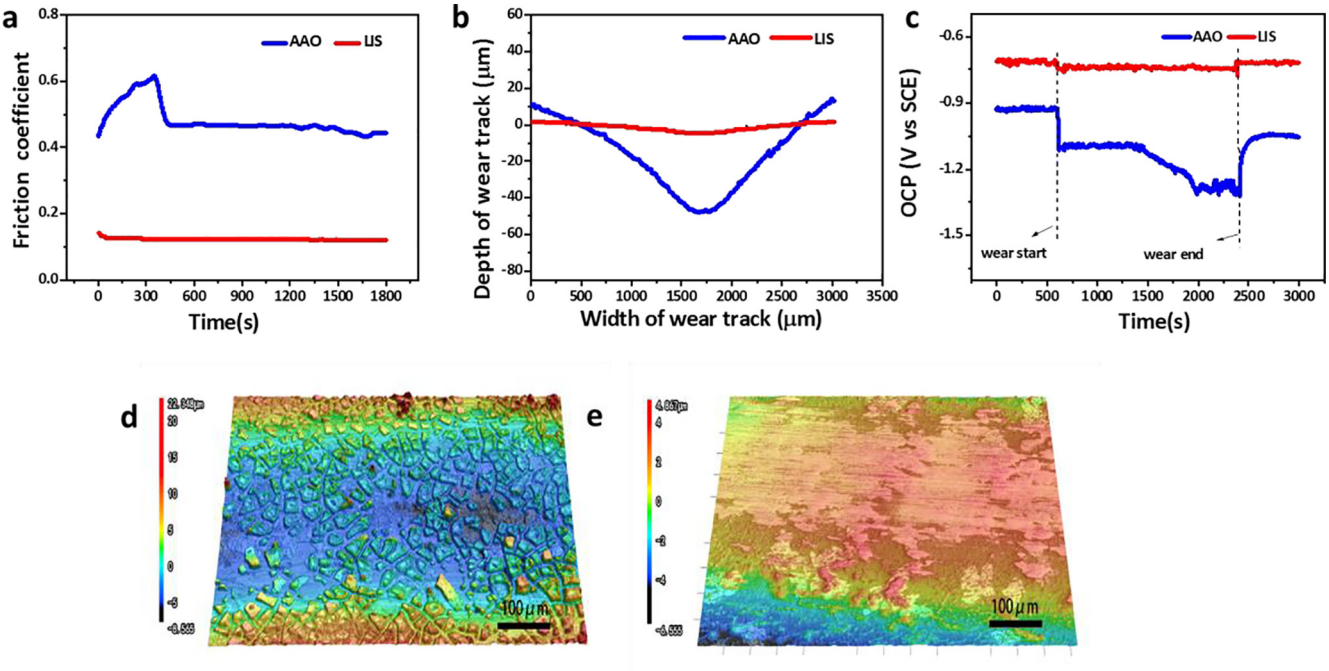

Fig. 7. Tribological behaviors of bare AAO and LIS: (a) friction coefficient during sliding, (b) depth of wear track and (c) open circuit potential during sliding; CLSM image of (d) worn bare AAO and (e) worn LIS after wearing for 1800 s.

4. Conclusions

A durable LIS was developed by infusing mineral oil lubricant into high-aspect-ratio AAO nanochannels (50 μm thick) using an effective vacuum impregnation method. The full lubricant infusion was visualized by cryo-SEM and confirmed by weighing. From the contact angle and sliding measurements, the LIS specimens showed a better water repellency than the bare AAO substrates, especially after a fluoroalkyl silane treatment. The combination of a relatively thick nanoporous substrate and abundant lubricant stored in the pores was advantageous for the corrosion resistance and self-healing property of LIS. EIS tests showed that the impedance moduli in the low-frequency region ($IZI_{0.01Hz}$) remained stable at $4 \times 10^8\,\Omega\,cm^2$ for the LIS immersed in NaCl solution for 85 days. The PDP results demonstrated the self-healing ability of LIS whose corrosion current density barely changed and remained at $2.99 \times 10^{-10}\,A\,cm^{-2}$ even after being cracked. Cryo-SEM observation provided insights into the self-healing process in which the lubricant around the surface micro-cracks flowed to the crack and covered the exposed aluminum substrate. Under tribological conditions, the low friction coefficient (0.12), the low depth of wear track (4.5 μm) and the well-preserved surface morphology indicated the excellent mechanical durability of the LIS. Using deep nanochannels as lubricant reservoirs, the LIS introduced in this study exhibited remarkable corrosion resistance and mechanical durability, which may contribute to the design of LIS for applications in high demanding environments.

Acknowledgement

This work is supported by National Natural Science Foundation of China (No. 51771029), the Beijing Nova Program (No. Z171100001117076) and the 111 Project (No.B170003).

Appendix A. Supplementary data

Supplementary data to this article can be found online at https://doi.org/10.1016/j.cej.2019.02.163.

References

[1] X. Li, D. Zhang, Z. Liu, Z. Li, C. Du, C. Dong, Share corrosion data, Nature 527 (2015) 441–442.
[2] S. Jia, X. Lu, S. Luo, Y. Qing, N. Yan, Y. Wu, Efficiently texturing hierarchical epoxy layer for smart superhydrophobic surfaces with excellent durability and exceptional stability exposed to fire, Chem. Eng. J. 348 (2018) 212–223.
[3] Y.C. Liu, W.J. Huang, S.H. Wu, L. Mei, J.M. Yeh, H.H. Chen, Excellent superhydrophobic surface and anti-corrosion performance by nanostructure of discotic columnar liquid crystals, Corros. Sci. 138 (2018) 1–7.
[4] B. Zhang, J. Li, X. Zhao, X. Hu, L. Yang, N. Wang, Y. Li, B. Hou, Biomimetic one step fabrication of manganese stearate superhydrophobic surface as an efficient barrier against marine corrosion and Chlorella vulgaris -induced biofouling, Chem. Eng. J. 306 (2016) 441–451.
[5] T.S. Wong, S.H. Kang, S.K. Tang, E.J. Smythe, B.D. Hatton, A. Grinthal, J. Aizenberg, Bioinspired self-repairing slippery surfaces with pressure-stable omniphobicity, Nature 477 (2011) 443.
[6] X. He, W. Qiang, C. Du, Q. Shao, X. Zhang, Y. Deng, Modification of lubricant infused porous surface for low-voltage reversible electrowetting, J. Mater. Chem. A (2017).
[7] X. Huang, J.D. Chrisman, N.S. Zacharia, Omniphobic slippery coatings based on lubricant-infused porous polyelectrolyte multilayers, ACS Macro Lett. 2 (2013) 826–829.
[8] D.J. Preston, Y. Song, Z. Lu, D.S. Antao, E.N. Wang, Design of lubricant infused surfaces, ACS Appl. Mater. Inter. (2017) 42383–42392.
[9] C. Zhang, B. Zhang, H. Ma, Z. Li, X. Xiao, Y. Zhang, X. Cui, C. Yu, M. Cao, L. Jiang, Bioinspired pressure-tolerant asymmetric slippery surface for continuous self-transport of gas bubbles in aqueous environment, ACS Nano 12 (2018) 2048–2055.
[10] X.Q. Wang, C.D. Gu, L.Y. Wang, J.L. Zhang, J.P. Tu, Ionic liquids-infused slippery surfaces for condensation and hot water repellency, Chem. Eng. J. 343 (2018) 561–571.
[11] Q. Wei, C. Schlaich, S. Prévost, A. Schulz, C. Böttcher, M. Gradzielski, Z. Qi, R. Haag, C.A. Schalley, Supramolecular polymers as surface coatings: rapid fabrication of healable superhydrophobic and slippery surfaces, Adv. Mater. 26 (2014) 7358–7364.
[12] F. Schellenberger, J. Xie, N. Encinas, A. Hardy, M. Klapper, P. Papadopoulos, H.J. Butt, D. Vollmer, Direct observation of drops on slippery lubricant-infused surfaces, Soft Matter 11 (2015) 7617–7626.
[13] P. Wang, T. Li, D. Zhang, Fabrication of non-wetting surfaces on zinc surface as corrosion barrier, Corros. Sci. 128 (2017) 110–119.
[14] T. Xiang, M. Zhang, H.R. Sadig, Z. Li, M. Zhang, C. Dong, L. Yang, W. Chan, C. Li, Slippery liquid-infused porous surface for corrosion protection with self-healing property, Chem. Eng. J. 345 (2018) 147–155.
[15] Y.H. Yeong, C. Wang, K.J. Wynne, M.C. Gupta, Oil-infused superhydrophobic silicone material for low ice adhesion with long-term infusion stability, ACS Appl. Mater. Inter. 8 (2016) 32050–32059.
[16] C. Wei, G. Zhang, Q. Zhang, X. Zhan, F. Chen, Silicone oil-infused slippery surfaces based on sol-gel process-induced nanocomposite coatings: a facile approach to highly stable bioinspired surface for biofouling resistance, ACS Appl. Mater. Inter. 8 (2016) 34810–34819.
[17] K. Golovin, S.P. Kobaku, D.H. Lee, E.T. DiLoreto, J.M. Mabry, A. Tuteja, Designing durable icephobic surfaces, Sci. Adv. 2 (2016) e1501496.
[18] S. Sett, X. Yan, G. Barac, L.W. Bolton, N. Miljkovic, Lubricant-infused surfaces for low-surface-tension fluids: promise versus reality, ACS Appl. Mater. Inter. 9 (2017) 36400–36408.
[19] S. Yuan, Z. Li, L. Song, H. Shi, S. Luan, J. Yin, A Liquid-infused poly(styrene-b-isobutylene-b-styrene) microfiber coating prevents biofilm attachment and thrombosis, ACS Appl. Mater. Inter. 8 (2016) 21214–21220.
[20] S. Sunny, N. Vogel, C. Howell, T.L. Vu, J. Aizenberg, Lubricant-infused nanoparticulate coatings assembled by layer-by-layer deposition, Adv. Funct. Mater. 24 (2015) 6658–6667.
[21] M. Liu, Y. Hou, J. Li, L. Tie, Z. Guo, Transparent slippery liquid-infused nanoparticulate coatings, Chem. Eng. J. 337 (2018) 462–470.
[22] S. Rowthu, P. Hoffmann, Perfluoropolyether-impregnated mesoporous alumina composites overcome the dewetting-tribological properties trade-off, ACS Appl. Mater. Inter. 10 (2018) 10560–10570.
[23] D. Zhang, L. Wang, H. Qian, X. Li, Superhydrophobic surfaces for corrosion protection: a review of recent progresses and future directions, J. Coat. Technol. Res. 13 (2016) 11–29.
[24] F. Zhang, P. Ju, M. Pan, D. Zhang, Y. Huang, G. Li, X. Li, Self-healing mechanisms in smart protective coatings: a review, Corros. Sci. (2018).
[25] W. Sun, L. Wang, Z. Yang, S. Li, T. Wu, G. Liu, Fabrication of polydimethylsiloxane-derived superhydrophobic surface on aluminium via chemical vapour deposition technique for corrosion protection, Corros. Sci. 128 (2017) 176–185.
[26] M. Muschi, B. Brudieu, J. Teisseire, A. Sauret, Drop impact dynamics on slippery liquid-infused porous surfaces: influence of oil thickness, Soft Matter 14 (2018) 1100–1107.
[27] J.H. Kim, J.P. Rothstein, Droplet impact dynamics on lubricant-infused superhydrophobic surfaces: the role of viscosity ratio, Langmuir 32 (2016).
[28] C. Lee, H. Kim, Y. Nam, Drop impact dynamics on oil-infused nanostructured surfaces, Langmuir 30 (2014) 8400–8407.
[29] C. Howell, T.L. Vu, C.P. Johnson, X. Hou, O. Ahanotu, J. Alvarenga, D.C. Leslie, O. Uzun, A. Waterhouse, P. Kim, Stability of surface-immobilized lubricant interfaces under flow, Chem. Mater. 27 (2016) 557762294.
[30] M. Tenjimbayashi, R. Togasawa, K. Manabe, T. Matsubayashi, T. Moriya, M. Komine, S. Shiratori, Liquid-infused smooth coating with transparency, super durability, and extraordinary hydrophobicity, Adv. Funct. Mater. 26 (2016) 6693–6702.
[31] R. Pant, S.K. Ujjain, A.K. Nagarajan, K. Khare, Enhanced slippery behavior and stability of lubricating fluid infused nanostructured surfaces, Eur. Phys. J. Appl. Phys. 75 (2016).
[32] Q. Liu, Y. Yang, M. Huang, Y. Zhou, Y. Liu, X. Liang, Durability of a lubricant-infused Electrospray Silicon Rubber surface as an anti-icing coating, Appl. Surf. Sci. 346 (2015) 68–76.
[33] I. Mohammadi, S. Ahmadi, A. Afshar, Effect of pulse current parameters on the mechanical and corrosion properties of anodized nanoporous aluminum coatings, Mater. Chem. Phys. 183 (2016) 490–498.
[34] E. Huttunen-Saarivirta, E. Isotahdon, J. Metsäjoki, T. Salminen, L. Carpén, H. Ronkainen, Tribocorrosion behaviour of aluminium bronze in 3.5 wt% NaCl solution, Corros. Sci. (2018).
[35] C. Boulesteix, V. Kolarik, F. Pedraza, Steam oxidation of aluminide coatings under high pressure and for long exposures, Corros. Sci. (2018).
[36] A. López-Ortega, J.L. Arana, E. Rodríguez, R. Bayón, Corrosion, wear and tribocorrosion performance of a thermally sprayed aluminum coating modified by plasma electrolytic oxidation technique for offshore submerged components protection, Corros. Sci. 143 (2018) 258–280.
[37] G.S. Lee, J.H. Choi, C.C. Yong, D.B. Sang, Y.Z. Lee, Tribological effects of pores on an anodized Al alloy surface as lubricant reservoir, Curr. Appl. Phys. 11 (2011) S182–S186.
[38] J. Lee, S. Shin, Y. Jiang, C. Jeong, H.A. Stone, C. Choi, Oil-impregnated nanoporous oxide layer for corrosion protection with self-healing, Adv. Funct. Mater. 27 (2017).
[39] T. Song, Q. Liu, J. Liu, W. Yang, R. Chen, X. Jing, K. Takahashi, J. Wang, Fabrication of super slippery sheet-layered and porous anodic aluminium oxide surfaces and its anticorrosion property, Appl. Surf. Sci. 355 (2015) 495–501.
[40] P. Huang, A. Somers, P.C. Howlett, M. Forsyth, Film formation in trihexyl(tetradecyl)phosphonium diphenylphosphate ([P6,6,6,14][dpp]) ionic liquid on AA5083 aluminium alloy, Surf. Coat. Technol. 303 (2016) 385–395.
[41] O.P. Oladijo, M.O. Bodunrin, K. Sobiyi, N.B. Maledi, K. Alaneme, Investigating the self-healing behaviour of under-aged and 60Sn-40Pb alloy reinforced aluminium hybrid composites, Thin Solid Films (2016).
[42] G. Lee, D. Cho, J. Kim, H. Kim, Y.C. Choi, S.D. Bu, Y. Lee, Lubricating layer formed

on porous anodic alumina template due to pore effect at water lubricated sliding and its properties, Thin Solid Films 521 (2012) 3–6.
[43] S. Anand, A.T. Paxson, R. Dhiman, J.D. Smith, K.K. Varanasi, Enhanced condensation on lubricant-impregnated nanotextured surfaces, ACS Nano 6 (2012) 10122.
[44] V. Raspal, K.O. Awitor, C. Massard, E. Feschet-Chassot, R.S. Bokalawela, M.B. Johnson, Nanoporous surface wetting behavior: the line tension influence, Langmuir 28 (2012) 11064–11071.
[45] K. Rykaczewski, T. Landin, M.L. Walker, J.H.J. Scott, K.K. Varanasi, Direct imaging of complex nano- to microscale interfaces involving solid, liquid, and gas phases, ACS Nano 6 (2012) 9326–9334.
[46] M. Zheng, M. Sakairi, H. Jha, Influence of desiccation procedures on the surface wettability and corrosion resistance of porous aluminium anodic oxide films, Corros. Sci. 55 (2012) 332–338.
[47] J.J. Suay, E. Gimenez, T. Rodrıguez, K. Habbib, J.J. Saura, Characterization of anodized and sealed aluminium by EIS, Corros. Sci. 45 (2003) 611–624.
[48] N. Hu, X. Dong, X. He, J.F. Browning, D.W. Schaefer, Effect of sealing on the morphology of anodized aluminum oxide, Corros. Sci. 97 (2015) 17–24.
[49] L. Wen, Y. Wang, Y. Zhou, J. Ouyang, L. Guo, D. Jia, Corrosion evaluation of microarc oxidation coatings formed on 2024 aluminium alloy, Corros. Sci. 52 (2010) 2687–2696.
[50] S. Touzain, Some comments on the use of the EIS phase angle to evaluate organic coating degradation, Electrochim. Acta 55 (2010) 6190–6194.
[51] Y. Zuo, R. Pang, W. Li, J.P. Xiong, Y.M. Tang, The evaluation of coating performance by the variations of phase angles in middle and high frequency domains of EIS, Corros. Sci. 50 (2008) 3322–3328.
[52] L.B. Boinovich, A.M. Emelyanenko, A.D. Modestov, A.G. Domantovsky, A.A. Shiryaev, K.A. Emelyanenko, O.V. Dvoretskaya, A.A. Ganne, Corrosion behavior of superhydrophobic aluminum alloy in concentrated potassium halide solutions: when the specific anion effect is manifested, Corros. Sci. 112 (2016) 517–527.
[53] U. Trdan, T. Sano, D. Klobčar, Y. Sano, J. Grum, R. Šturm, Improvement of corrosion resistance of AA2024-T3 using femtosecond laser peening without protective and confining medium, Corros. Sci. 143 (2018) 46–55.
[54] S. Wang, H. Peng, Z. Shao, Q. Zhao, N. Du, Sealing of anodized aluminum with phytic acid solution, Surf. Coat. Technol. 286 (2016) 155–164.
[55] D. Zhang, H. Qian, L. Wang, X. Li, Comparison of barrier properties for a superhydrophobic epoxy coating under different simulated corrosion environments, Corros. Sci. 103 (2016) 230–241.
[56] V. Moutarlier, M.P. Gigandet, B. Normand, J. Pagetti, EIS characterisation of anodic films formed on 2024 aluminium alloy, in sulphuric acid containing molybdate or permanganate species, Corros. Sci. 47 (2005) 937–951.
[57] R. Jeltes, W.A.M.D. Tonkelaar, Gas chromatography versus infra-red spectrometry for determination of mineral oil dissolved in water, Water Res. 6 (1972) 271–278.
[58] A.C. Vieira, L.A. Rocha, N. Papageorgiou, S. Mischler, Mechanical and electrochemical deterioration mechanisms in the tribocorrosion of Al alloys in NaCl and in NaNO3 solutions, Corros. Sci. 54 (2012) 26–35.
[59] D. Landolt, S. Mischler, M. Stemp, Electrochemical methods in tribocorrosion: a critical appraisal, Electrochim. Acta 46 (2001) 3913–3929.